Biochemical and Biophysical Research Communications 517 (2019) 703–708

Contents lists available at ScienceDirect

Biochemical and Biophysical Research Communications

journal homepage: www.elsevier.com/locate/ybbrc

Physicochemical factors that affect electroporation of lung cancer and normal cell lines

Hong Bae Kim [a, 1], Seho Lee [b, 1], Yiming Shen [c], Pan-Dong Ryu [c], Yunmi Lee [d], Jong Hoon Chung [a], Chang Kyu Sung [e, **], Ku Youn Baik [f, *]

[a] Department of Biosystems & Biomaterials Science and Engineering, Seoul National University, Seoul, 08826, South Korea
[b] Department of Brain and Cognitive Engineering, Korea University, Seoul, 02841, South Korea
[c] Department of Veterinary Pharmacology, College of Veterinary Medicine and Research Institute for Veterinary Science, Seoul National University, Seoul, 08826, South Korea
[d] Department of Chemistry, Kwangwoon University, Seoul, 01897, South Korea
[e] Department of Radiology, Seoul National University College of Medicine, Seoul, 07061, South Korea
[f] Department of Electrical and Biological Physics, Kwangwoon University, Seoul, 01897, South Korea

ARTICLE INFO

Article history:
Received 24 July 2019
Accepted 30 July 2019
Available online 3 August 2019

Keywords:
Electroporation
Electropermeabilization
Membrane stiffness
Resting transmembrane potential
Lipid cholesterol ration

ABSTRACT

Electroporation is used for cancer therapy to efficiently destroy cancer tissues by transferring anticancer drugs into cancer cells or by irreversible tumor ablation without resealing pores. There is growing interest in the electroporation method for the treatment of lung cancer, which has the highest mortality rate among cancers. Improving the cancer cell selectivity has the potential to expand its use. However, the factors that influence the cell selectivity of electroporation are debatable. We aimed to identify the important factors that influence the efficiency of electroporation in lung cells. The electropermeabilization of lung cancer cells (H460, A549, and HCC1588) and normal lung cells (MRC5, WI26 and L132) was evaluated by the transfer of fluorescence dyes. We found that membrane permeabilization increased as cell size, membrane stiffness, resting transmembrane potential, and lipid cholesterol ratio increased. Among them, lipid composition was found to be the most relevant factor in the electroporation of lung cells. Our results provide insight into the differences between lung cancer cells and normal lung cells and provide a basis for enhancing the sensitivity of lung cancers cells to electroporation.

1. Introduction

The electroporation technique utilizes high-magnitude electric pulses to induce cell membrane permeability [1]. This technique is used for tumor therapy to efficiently destroy cancer tissues by transferring anticancer drugs into cancer cells or by irreversible tumor ablation without resealing pores [2]. Electrochemotherapy is currently used in many cancer centers as a safe and efficient method, and the use of calcium instead of anticancer drugs is being investigated in clinical trials to reduce side effects [3]. Irreversible electroporation has been used in clinical settings since 2008, especially for the treatment of locally advanced pancreatic cancer, and demonstrates suitable safety and palliation [4,5]. For both approaches, cancer cell selectivity to electric pulses can improve the safety of electroporation as a therapeutic tool.

There is debate regarding the factors that influence cell selectivity of electroporation. Some studies have indicated that the viability of cells after electric pulse applications is largely dependent on cell types whereas the electropermeabilization is not [6,7]. However, other reports have suggested that there is selectivity between cancer and normal cells [8–11]. Pore size and density are dependent on the applied electric field strength, pulse duration, and pulse number. Additionally, physical properties of target cells, such as cell size, mechanical properties, and electrical properties are important. In the simplest mechanical model that considers the lipid membrane as a uniform isotropic capacitor, cell size is the main determinant of the effect of electroporation [11–13]. However, experimental results have shown that there should be other factors which are more powerful than cell size [7]. Mechanical factors, such as membrane stiffness or fluidity, were reported to

* Corresponding author.
** Corresponding author.
E-mail addresses: sckmd@hanmail.net (C.K. Sung), kybaik@kw.ac.kr (K.Y. Baik).
[1] Both authors contribute equally to this work.

https://doi.org/10.1016/j.bbrc.2019.07.119
0006-291X/

affect the size of pores and the resealing time [14]. Electrical factors, such as the resting transmembrane potential difference (TMP), affect the threshold voltage and induce anisotropic electroporation [15–17]. The cholesterol content could also explain differences in susceptibility [18,19].

In this study, we investigated the correlation between cellular physical factors and electroporation efficiency. Briefly, electroporation efficiency was assessed by membrane permeabilization based on the fluorescence intensity of propidium iodide (PI) in cells, as determined by flow cytometry. We examined six human lung cell lines, including three cancer cell lines (H460, A549, and HCC1588) and three normal cell lines (MRC5, WI26, and L132). Since lung cancer has the highest mortality rate among cancers worldwide, it is necessary to develop efficient treatment methods, and there is growing interest in the electroporation method, which induces a weak immune response [20]. Cell size, membrane stiffness, resting TMP, and membrane composition of these cells were analyzed separately. The relationships between these properties and the efficiency of electroporation were examined, followed by discussion on the underlying mechanisms.

2. Materials and methods

2.1. Cell culture

Human lung cell lines were purchased from the Korean Cell Line Bank and maintained in DMEM (LM001-05; Welgene) supplemented with 10% FBS (A1500; RDTech) and 1% antibiotics (LS203-01; Welgene) at 37 °C in a humidified environment with 5% CO_2. At 24 h before the experiments, 2×10^5 cells were seeded in a Petri dish (35 mm in diameter). MRC5 and WI26 are fibroblast cell lines and the other four lines are of epithelial origin. H460 and A549 are carcinoma cells and HCC1588 is a squamous cancer cell line.

2.2. Electroporation procedure

To apply a certain electric field to cells on the dish, we used specially designed electrodes composed of parallel plates with gaps of 2.5 mm, as shown in Fig. 1. These parallel metal plates were coated with gold to avoid toxic metal ions from electrochemical reaction. Electroporation was performed in 1 ml of serum-free DMEM containing 50 μg/ml propidium iodide (PI; P4170, Sigma). Rectangular direct current pulses of 100 μs were sequentially applied 8 times at intervals of 100 m s with electric field strengths of 200, 300, 400, 500, 600, and 700 V/cm using a pulse generator (ECM 830; BTX.). Cells were then incubated for 5 min to allow the transfer of PI into cells through pores made. Then, adherent cells were washed three times with DPBS (LB001-02, Welgene) to eliminate extracellular PI. To quantitatively measure the PI fluorescence intensity per a cell, cells were harvested using 0.25% trypsin and washed three times with DPBS. Then, trypsinized cells were suspended in DPBS solution and analyzed by flow cytometry (BD FACSVerse™).

2.3. Flow cytometry

Cells were suspended in DPBS solution and the sheath flow was controlled to make the number of about 200 cells per second. Cells were gated by their forward scattering (FSC) and side scattering (SSC) as shown in Fig. 2(a). Voltage of PMT was controlled to make the control fluorescent intensity near $10^3.10^4$ cells in the gate were analyzed for one measurement, and the mean value was analyzed by BD FACSUITE Software. Forward scattering values obtained by flow cytometry were used to calculate cell sizes. The relative fluorescence intensity of each group to control was expressed as a ratio

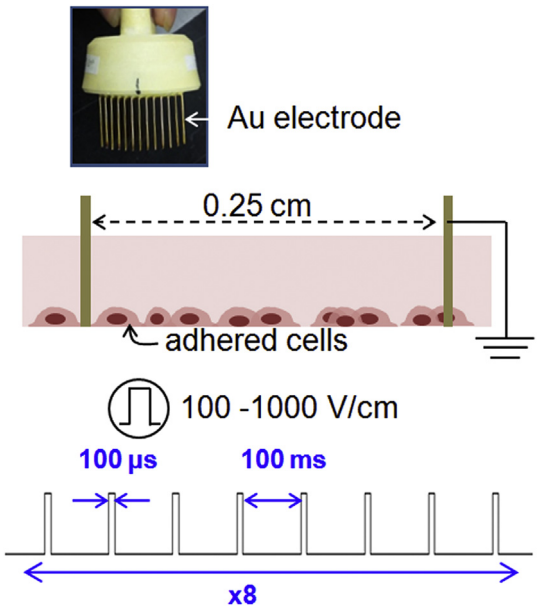

Fig. 1. Schematic diagram of the application of electric pulses to adherent mammalian cells. Electric pulses with durations of 100 μs at intervals of 100 ms were serially applied 8 times.

value. The MFI (mean fluorescence intensity) of PI was calculated as follows. Experiments were repeated four times.

$$\text{Relative PI MFI} = (\text{MFI}_{\text{SAMPLE}} - \text{MFI}_{\text{CONTROL}})/\text{MFI}_{\text{CONTROL}}$$

$$\text{Normalized PI MFI} = (\text{MFI}_{\text{SAMPLE}} - \text{MFI}_{\text{CONTROL}})/ \times (\text{MFI}_{\text{SATURATED}} - \text{MFI}_{\text{CONTROL}})$$

2.4. Measurement of membrane stiffness

Nano-indentation by atomic force microscopy (AFM; MFP-3D; Asylum Research Inc.) was used to calculate the cell membrane stiffness. V-shaped silicon nitride cantilevers (PMCL-TR800PB) were used with a regular four-sided pyramidal tip of open angle $\theta = 35°$. The spring constant was measured as $k = 476.83$ fN/nm, by analyzing the thermal resonant vibration. The deflection versus distance was calibrated by recording force curves of the cantilever on the bare cover glass in DPBS. Since cells have non-symmetric shape, the indentation measurement was applied only on the nucleus region of cells. Choosing this nucleus region has less effect from surface curvature and the bottom substrate. Cells that were cultivated on the cover glass (Mariendfeld GmbH & Co.KG in Germany) were placed under the cantilever, and the end of tip of cantilever was exactly positioned over the cell nucleus region using micromanipulator. Young's modulus was obtained by least square analysis with the Poisson ratio of 0.5 by Hertz model.

2.5. Patch clamp method

Patch clamp method was used to directly measure the resting trans-membrane potential difference. Cells were precipitated and bathed in a sag recording chamber (0.7 ml) with oxygenated extracellular recording solution containing (in mM): 126 NaCl, 26 $NaHCO_3$, 5 KCl, 1.2 NaH_2PO_4, 2.4 $CaCl_2$, 1.2 $MgCl_2$, and 10 glucose at a rate of 3–5 ml/min. The recording pipettes (PG52151-4; World Precision Instruments) were pulled by a two-step heat puller (PC-

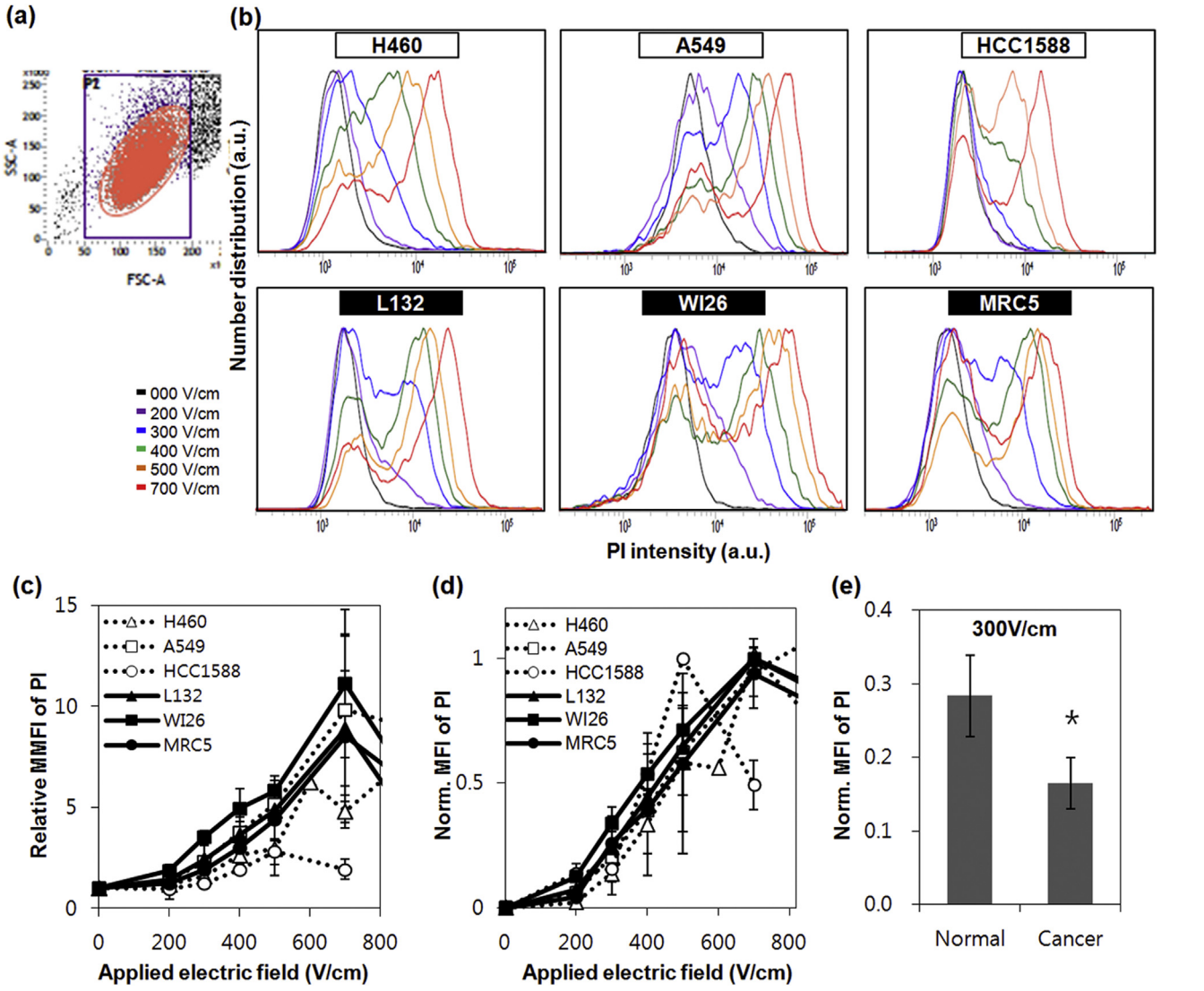

Fig. 2. Electropermeabilization of three human lung cancer cell lines (H460, A549, and HCC1588) and three human lung normal cell lines (L132, WI26, and MRC5). (a) Cells were gated by their FSC and SSC values. (b) Distributions of PI-MFI after the application of electric pulses of different voltages. (c) PI MFI relative to each control. (d) Normalized PI MFI relative to each cell. (e) Average normalized PI MFI of three normal and three cancer cells at 300 V/cm (*: $P < 0.05$).

10; Narishige) and filled with K-gluconate-rich solution composed of the following (in mM): 135 K-gluconate, 5 KCl, 20 HEPES, 0.5 $CaCl_2$, 5 EGTA, and 5 ATP-Mg. Its pH was adjusted with KOH to 7.2–7.3 (liquid junction potential, −14.4 mV). The cells were selected and the resting membrane potential was recorded in the whole-cell current-clamp configuration through an Axopatch 200B (Axon Instruments, Foster City, CA). All signals were filtered at 1 kHz and digitized at 20 kHz (Digidata 1200B, pClamp 8 software; Axon Instruments) [21].

2.6. ^1H NMR spectroscopy

The lipid composition was measured by ^1H NMR analysis. The total lipids were extracted by the chloroform–methanol method [22] and the samples were dissolved in $CDCl_3$ solvent. ^1H NMR spectra were recorded on a Bruker AVANCE 600 MHz spectrometer. Chemical shifts are reported in ppm from tetramethylsilane, with the solvent resonance as internal standard ($CDCl_3$: δ 7.27 ppm). The NMR spectra are assigned with reference to the NMR lipid database [23].

2.7. Statistical analysis

Means and standard deviations were calculated. All of the experiments were repeated more than three times, and the standard deviations were plotted in the graph. An unpaired two-sided Student's *t*-test was performed by Excel, and it was considered statistically significant when $P < 0.05$ (*). The correlation coefficients were calculated as follows (HCC1588 cells were excluded, since the PI MFI value was too low compared to those for the other cell types):

$$\rho_{X,Y} = \frac{Cov(X,Y)}{\sigma_X \sigma_Y}$$

3. Result and discussion

Fig. 2(b) shows the distribution of cell counts for each condition. The peaks shifted to a higher PI MFI as the applied electric field increased. Fig. 2(c) shows that the relative PI MFI increased

according to the applied electric field strength for all cell lines. To normalize the results, the baseline MFI at 0 V/cm was set to 0 and the highest MFI at 700 or 800 V/cm was set to 1. Fig. 2(d) shows the normalized MFI values for the six cell lines. Fig. 2(c) and (d) show that the threshold voltages for membrane permeabilization by electric pulses did not differ substantially among the cells. Most cells showed an increase in MFI near 200 V/cm. However, cancer cell lines (shown as white dots in Fig. 2) had slightly weaker MFIs than normal cell lines (black filled dots) at a low electric field. Fig. 2(e) shows that the MFI at 300 V/cm was significantly different between cancer and normal cells. Unfortunately, the PI MFI was lower in cancer cells than in normal cells, indicating that the electroporation efficiency is lower in lung cancer cells.

To determine the factors that contribute to the differences in efficiency, we analyzed various physicochemical properties, including the cell size, membrane stiffness, resting TMP, and lipid membrane composition. All values were normalized to the average value for normal cells. Fig. 3(a) shows an optical image of each cell during cantilever-based AFM nano-indentation. There was variation in cell shapes and sizes. Since it was difficult to precisely measure cell sizes by microscopy, flow cytometry was used to examine cells that detached from the surface. Though cell shape on the flat surface was much different each other, we postulated that the height and length of cells could be determined by their innate volume. Fig. 3(b) shows that cancer cells were slightly smaller than normal cells in the forward scattering analysis based on the shadow area when cells flew through a laser spot. Fig. 3(c) summarizes membrane stiffness for normal and cancer cells. Membrane stiffness was significantly weaker for cancer cells than for normal cells. The adhesion property of cells may affect these measurements. As summarized in Fig. 3(d), the resting TMP was slightly lower in cancer cells than in normal cells, but there were large differences among cells. Fig. 3(e) shows that the lipid compositions of cells were nearly identical. However, when each peak area was normalized to the total peak area, we found that the ratio of cholesterol at $\delta = 0.7$ ppm was lower in cancer cells than in normal cells (Fig. 3(f)) [24].

Interestingly, all measured factors had a tendency similar to that of the normalized PI MFI shown in Fig. 2(e). Lung cancer cells had a slightly smaller size, significantly lower membrane stiffness, slightly lower resting TMP, and significantly lower cholesterol ratio. H460 and A549 are non-small-cell lung carcinoma cells, which are known to have small nuclei [25]. This may explain the slightly smaller cell size. A lower membrane stiffness and lower resting TMP are general cancer phenotypes [26,27]. A low cholesterol ratio is a unique property of lung cancer cells, distinct from other cancer types [28,29]. Since the trends of all the parameters were similar to that of the normalized PI MFI, it is difficult to identify the major determinants of the efficiency of electroporation. To identify significant determinants of the efficiency of electroporation, we plotted values for (1) cell size, (2) membrane stiffness, (3) resting TMP, and (4) cholesterol ratio, against the normalized PI MFI for each cell, as shown in Fig. 4. The correlation coefficients were calculated and inserted in the graphs. As expected, all four factors were positively correlated with normalized PI-MFI (Fig. 4(a–d)).

We selected an NMR peak value at 5.2 ppm, which represented double bonds in the fatty acid chain. The normalized peak area to the total area did not differ between cancer and normal cell lines.

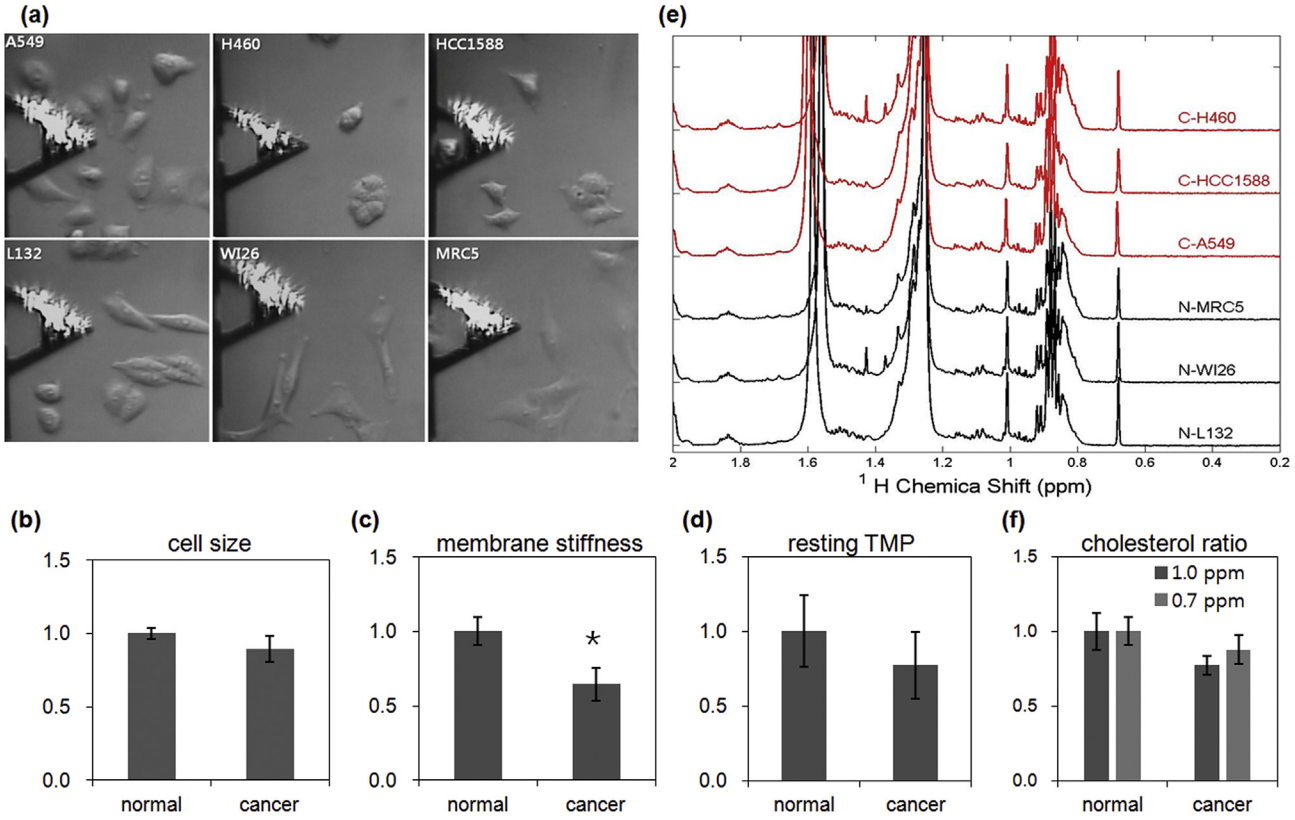

Fig. 3. Physical parameters for six lung cell lines and differences between normal and cancer lung cell lines. (a) Optical microscopy of each cell line using an AFM cantilever approach. (b) ^{1}H NMR spectroscopy of lipids extracted from whole cells. (c) Average size of normal and cancer cell lines. (d) Average cellular stiffness of normal and cancer cell lines. (e) Average trans-membrane potential of normal and cancer cell lines. (f) Average ratio of cholesterol to whole lipids of normal and cancer cell lines. The peak areas at 0.7 and 1.0 ppm were calculated (*: $P < 0.05$).

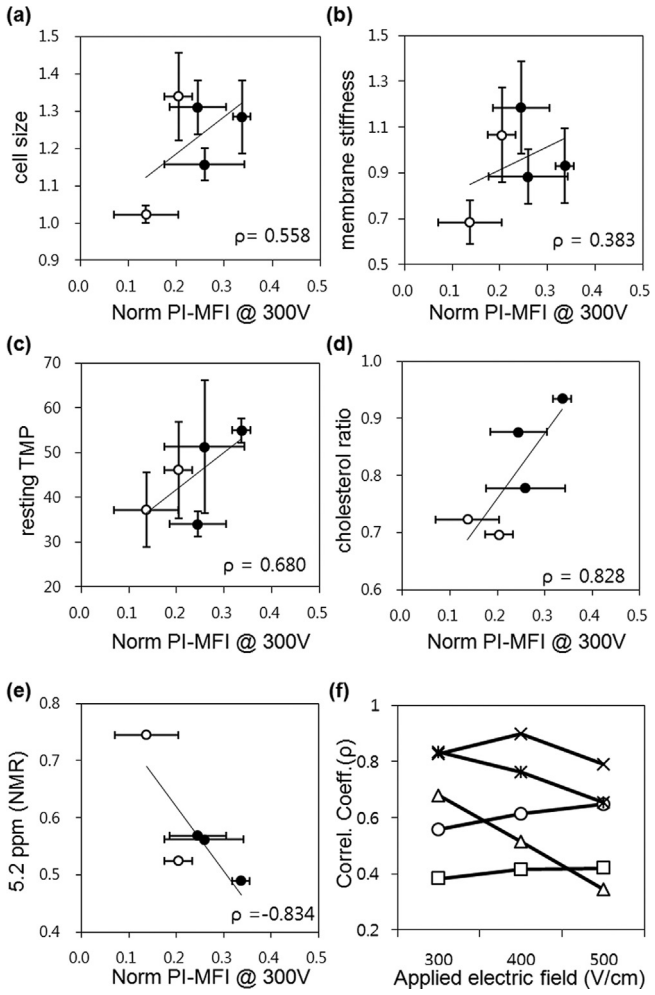

Fig. 4. Correlation coefficients for the relationships between normalized PI MFI and physical factors. The means and standard deviation were used; (a) cell size, (b) membrane stiffness, (c) trans-membrane potential, (d) cholesterol ratio, (e) ratio of double bonds in fatty acid chain. (f) The correlation coefficients were plotted according to applied electric field (*: $P < 0.05$).

However, there was a negative relationship with normalized PI-MFI (Fig. 4(e)). Membrane stiffness had the lowest and relative cholesterol had the highest correlation coefficient. Since correlation coefficients of less than +0.8 or greater than −0.8 are not considered significant, only lipid composition had a significant relationship with electroporation efficiency. To confirm these relationships at other applied electric fields, we repeated the analyses at 300, 400, and 500 V/cm, where PI MFI values were under saturation. Fig. 4(f) shows the correlation coefficients according to field strength. Relative cholesterol values exhibited the highest correlations in all cases, and the coefficients for membrane stiffness and cell size did not change according to the applied electric field. Interestingly, the coefficients for resting TMP and double bond ratio decreased as the applied electric field increased.

The low correlation between cell size and PI MFI implies that the simple lipid vesicle model of a cell is not sufficient. Inconsistent results regarding the role of cell size in electroporation have been reported. As predicted by a simple mechanical model, a study has shown that cell size is a determinant of the electroporation efficiency for three-dimensional hydrogel cell culture [11]. However, another report has shown that cell size has no relationship with the electroporation of trypsinized cells [7]. Our experiments were executed in two-dimensional adhesion states, so the effect of size can be different. Additionally, our experimental analysis is expected to have large errors because cell size measurements were not obtained when cells were attached to the substrate. The effects of size or morphology should be investigated further in a tissue model to make it close to the actual medical situation.

The resting TMP had a slightly higher correlation with MFI, but the correlation was not significant. Previous experimental studies have shown that there is no relationship between resting TMP and fluorescent molecule transfer through the membrane [30]. However, the change in the correlation according to the external applied electric field confirms that the resting TMP affected the threshold voltage. As the induced TMP caused by externally applied electric pulses is superimposed on the resting TMP of the cell, the side of the cell facing the anode is hyperpolarized, while the side facing the cathode is depolarized [31]. This implies that the resting TMP can affect the threshold voltage that triggers electroporation, especially when the induced TMP is close to the threshold voltage [32].

The least correlated factor, membrane stiffness measured by AFM, generally reflects the stiffness of actin filaments under the membrane. Previous studies have reported that actin fibers are disrupted and reorganized by electric pulses and that apoptosis and necrosis in response to electric pulses decrease when actin is disrupted [33,34]. Some studies have indicated that cytoskeletons play a role in electroporation by expediting pore resealing [35,36]. However, the effect of actins on electropermeabilization itself was not strongly highlighted, which might have little relationship as our data show.

Other factors, including the cholesterol ratio and double bond ratio in fatty acids, are related to membrane fluidity, a mechanical property of a cell membrane. A high cholesterol ratio makes the membrane stiffer, and a high double bond ratio in fatty acids makes the membrane more fluidic [37]. There are conflicting findings regarding the effect of membrane fluidity on electroporation. On the one hand, the exposure of cells to low temperature or to chemicals inducing disorder increased the voltage required for successful electroporation [18,38,39]. On the other hand, cells with less fluid membranes were permeabilized at lower voltages than those of cells with more fluid membranes [14]. Our experimental results suggest that less fluid membranes (high cholesterol and low double bond contents) are more easily electropermeabilized. This result is not consistent with those of a previous study in which a chemical was used to remove cholesterol [18]. It could be lung tissue-specific, since cholesterol has a special role as a surfactant in the lung [40]. The electric field dependency of the double bond ratio implies that cholesterol and double bond ratios are involved via different mechanisms. Compared with changes in the overall lipid composition, the membrane domain structure is likely more responsible for the observed differences in electroporation behavior [41].

In summary, we identified determinants of the efficiency of electroporation in lung cells by analyzing the correlations between physicochemical properties of cells and electropermeabilization of a fluorescent dye. We found that the electroporation efficiency increased as cell size, membrane stiffness, resting TMP, and cholesterol level increased. Actually, the effect of each factor could not be analyzed by a simple comparison, because electropermeabilization was not determined by one factor as our analysis showed. The combination analysis of factors or the experimental regulation of factors should be necessary for more clear understanding of the effect of each factor. Although our analysis does not cover such tries, we can figure out the relative influence of each factor on electroporation in lung cells. Our findings suggest that the modulation of these factors is expected to enhance the efficiency or selectivity of electroporation in lung cancer cells that are less sensitive to applied electric pulses on its own.

Acknowledgements

This work was supported by the Innovative Technology Development Project of 2017 (S2459501) that was funded by the Ministry of Small and Medium-sized Enterprises and Startups (MSS, Korea).

Transparency document

Transparency document related to this article can be found online at https://doi.org/10.1016/j.bbrc.2019.07.119.

References

[1] J.M. Crowley, Electrical breakdown of biomolecular lipid membranes as an electromechanical instability, Biophys. J. 13 (1973) 711–724.
[2] M. Breton, L.M. Mir, Microsecond and nanosecond electric pulses in cancer treatments, Bioelectromagnetics 33 (2012) 106–123.
[3] C.C. Plaschke, J. Gehl, H.H. Johannesen, B.M. Fischer, A. Kjaer, A.F. Lomholt, I. Wessel, Calcium electroporation for recurrent head and neck cancer: a clinical phase I study, Laryngoscope Investig. Otolaryngol. 4 (1) (2019) 49–56.
[4] M. Bower, L. Sherwood, Y. Li, R. Martin, Irreversible electroporation of the pancreas: definitive local therapy without systemic effects, J. Surg. Oncol. 104 (1) (2011) 22–28.
[5] H.J. Scheffer, K. Nielsen, M.C. de Jong, A.A. van Tilborg, J.M. Vieveen, A.R. Bouwman, S. Meijer, C. van Kuijk, P.M. van den Tol, M.R. Meijerink, Irreversible electroporation for nonthermal tumor ablation in the clinical setting: a systematic review of safety and efficacy, J. Vasc. Interv. Radiol. 25 (7) (2014) 997–1011.
[6] M.J. O'Hare, M.G. Ormerod, P.R. Imrie, J.H. Peacock, W. Asche, Electropermeabilization and electrosensitivity of different types of mammalian cells, Electroporation and Electrofusion Cell Biol. 319 (1989) 330.
[7] M. Čemazar, T. Jarm, M. Miklavčič, A.M. Lebar, A. Ihan, N.A. Kopitar, Effect of electric field intensity on electropermeabilization and electrosensitivity of various tumor-cell lines in vitro, Electro- Magnetobiol. 17 (2) (1998) 263–272.
[8] W. Yang, Y.H. Wu, D. Yin, H.P. Koeffler, D.E. Sawcer, P.T. Vernier, M.A. Gundersen, Differential sensitivities of malignant and normal skin cells to nanosecond pulsed electric fields, Technol. Cancer Res. Treat. 10 (3) (2011) 281–286.
[9] S.K. Frandsen, M.B. Krüger, U.M. Mangalanathan, T. Tramm, F. Mahmood, I. Novak, J. Gehl, Normal and malignant cells exhibit differential responses to calcium electroporation, Cancer Res. 77 (2017) 4389–4401.
[10] K.L. Hoejholt, T. Mužić, S.D. Jensen, L.T. Dalgaard, M. Bilgin, J. Nylandsted, T. Heimburg, S.K. Frandsen, J. Gehl, Calcium electroporation and electrochemotherapy for cancer treatment: importance of cell membrane composition investigated by lipidomics, calorimetry and in vitro efficacy, Sci. Rep. 9 (2019) 4758.
[11] J.W. Ivey, E.L. Latouche, M.B. Sano, J.H. Rossmeisl, R.V. Davalos, S.S. Verbridge, Targeted cellular ablation based on the morphology of malignant cells, Sci. Rep. 5 (2015), 17157.
[12] H. Shagoshtasbi, P. Deng, Y.K. Lee, A nonlinear size-dependent equivalent circuit model for single-cell electroporation on microfluidic chips, J. Lab. Autom. 20 (2015) 481–490.
[13] A. Agarwal, I. Zudans, E.A. Weber, J. Olofsson, O. Orwar, S.G. Weber, Effect of cell size and shape on single-cell electroporation, Anal. Chem. 79 (2007) 3589–3596.
[14] M. Kanduser, M. Sentjurc, D. Miklavcic, Cell membrane fluidity related to electroporation and resealing, Eur. Biophys. J. 35 (2006) 196–204.
[15] B. Valic, M. Pavlin, D. Miklavcic, The effect of resting transmembrane voltage on cell electroporation: a numerical analysis, Bioelectrochemistry 63 (1–2) (2004) 311–315.
[16] E.J. Aiken, B.G. Kilberg, S. Yu, S.C. Hagness, J.H. Booske, Ionomycin-induced changes in membrane potential alter electroporation outcomes in HL60 cells, Biophys. J. 114 (12) (2018) 2875–2886.
[17] S.M. Kennedy, E.J. Aiken, K.A. Beres, A.R. Hahn, S.J. Kamin, S.C. Hagness, J.H. Booske, W.L. Murphy, Cationic peptide exposure enhances pulsed-electric-field-mediated membrane disruption, PLoS One 9 (3) (2014), e92528.
[18] J.C. Cantu, M. Tarango, H.T. Beier, B.L. Ibey, The biological response of cells to nanosecond pulsed electric fields is dependent on plasma membrane cholesterol, Biochim. Biophys. Acta Biomembr. 1858 (11) (2016) 2636–2646.
[19] I. van Uitert, S. Le Gac, A. van den Berg, The influence of different membrane components on the electrical stability of bilayer lipid membranes, Biochim. Biophys. Acta 1798 (2010) 21–31.
[20] D.A. Dean, Electroporation of the vasculature and the lung, DNA Cell Biol. 22 (12) (2003) 797–806.
[21] J.E. Yang, M.S. Song, Y.M. Shen, P.D. Ryu, S.Y. Lee, The role of KV7.3 in regulating osteoblast maturation and mineralization, Int. J. Mol. Sci. 17 (3) (2016) 407.
[22] E.G. Baligh, W.J. Dyer, A rapid method of total lipid extraction and purification, Can. J. Biochem. Physiol. 37 (8) (1959) 911–917.
[23] R.K. Adosraku, G.T. Choi, V. Constantinou-Kokotos, M.M. Anderson, W.A. Gibbons, NMR lipid profiles of cells, tissues, and body fluids: proton NMR analysis of human erythrocyte lipids, J. Lipid Res. 35 (1994) 1925–1931.
[24] R. Khatun, H. Hunter, W. Magcalas, Y. Sheng, B. Carpick, M. Kirkitadze, Nuclear magnetic resonance (NMR) study for the detection and quantitation of cholesterol in HSV529 therapeutic vaccine candidate, Comput. Struct. Biotechnol. J. 15 (2017) 14–20.
[25] I. Petersen, The morphological and molecular diagnosis of lung cancer, Dtsch Arztebl Int 108 (31–32) (2011) 525–531.
[26] S. Suresh, Nanomedicine: elastic clues in cancer detection, Nat. Nanotechnol. 2 (12) (2007) 748–749.
[27] M. Yang, W.J. Brackenbury, Membrane potential and cancer progression, Front. Physiol. 4 (2013) 185.
[28] O.F. Kuzu, M.A. Noory, G.P. Robertson, The role of cholesterol in cancer, Cancer Res. 76 (8) (2016) 2063–2070.
[29] X. Lin, L. Lu, L. Liu, S. Wei, Y. He, J. Chang, X. Lian, Blood lipids profile and lung cancer risk in a meta-analysis of prospective, J. Clin. Lipidol. 11 (4) (2017) 1073–1081.
[30] M.N. Teruel, T. Meyer, Electroporation-induced formation of individual calcium entry sites in the cell body and processes of adherent cells, Biophys. J. 73 (4) (1997) 1785–1796.
[31] W. Frey, J.A. White, R.O. Price, P.F. Blackmore, R.P. Joshi, R. Nuccitelli, S.J. Beebe, K.H. Schoenbach, J.F. Kolb, Plasma membrane voltage changes during nanosecond pulsed electric field exposure, Biophys. J. 90 (10) (2006) 3608–3615.
[32] M. Kanduser, D. Miklavcic, Electroporation in biological cell and tissue: an overview, Food Eng. Ser. 1–37 (2009).
[33] A.G. Pakhomov, A. Xiao, O.N. Pakhomova, I. Semenov, M.A. Kuipers, B.L. Ibey, Disassembly of actin structures by nanosecond pulsed electric field is a downstream effect of cell swelling, Bioelectrochemistry 100 (2014) 88–95.
[34] G.L. Thompson, C. Roth, G. Tolstykh, M. Kuipers, B.L. Ibey, Role of cytoskeleton and elastic moduli in cellular response to nanosecond pulsed electric fields, in: Proc. SPIE 8585, Terahertz and Ultrashort Electromagnetic Pulses for Biomedical Applications, 2013, 85850 T.
[35] C. Blangero, M.P. Rols, J. Teissie, Cytoskeletal reorganization during electric-field-induced fusion of Chinese hamster ovary cells grown in monolayers, Biochim. Biophys. Acta 981 (2) (1989) 295–302.
[36] J. Teissie, M.P. Rols, Manipulation of cell cytoskeleton affects the lifetime of cell membrane electropermeabilization, Ann. NY Acad. Sci. 720 (1994) 98–110.
[37] E.J. Fernández-Pérez, F.J. Sepúlveda, C. Peters, D. Bascuñán, N.O. Riffo-Lepe, J. González-Sanmiguel, S.A. Sánchez, R.W. Peoples, B. Vicente, L.G. Aguayo, Effect of cholesterol on membrane fluidity and association of Aβ oligomers and subsequent neuronal damage: a double-edged sword, Front. Aging Neurosci. 10 (2018) 226.
[38] M.P. Rols, F. Dahhou, K.P. Mishra, J. Teissie, Control of electric field induced cell membrane permeabilization by membrane order, Biochemistry 29 (1990) 2960–2966.
[39] M. Kandušer, M. Šentjurc, D. Miklavčič, The temperature effect during pulse application on cell membrane fluidity and permeabilization, Bioelectrochemistry 74 (2008) 52–57.
[40] J.M. Andersson, C. Grey, M. Larsson, T.M. Ferreira, E. Sparr, Effect of cholesterol on the molecular structure and transitions in a clinical-grade lung surfactant extract, Proc. Natl. Acad. Sci. 114 (22) (2017), E4520.
[41] D. Lingwood, K. Simons, Lipid rafts as a membrane-organizing principle, Science 327 (2010) 46–50.